Journal of Pharmaceutical Analysis 12 (2022) 860–868

Contents lists available at ScienceDirect

Journal of Pharmaceutical Analysis

journal homepage: www.elsevier.com/locate/jpa

Original article

Discovery of pulmonary fibrosis inhibitor targeting TGF-β RI in *Polygonum cuspidatum* by high resolution mass spectrometry with in silico strategy

Huarong Xu [a], Jiameng Qu [a, b], Jian Wang [c], Kefei Han [a, b], Qing Li [a], Wenchuan Bi [d, **], Ran Liu [a, *]

[a] National and Local Joint Engineering Laboratory for Key Technology of Chinese Material Medica Quality Control, School of Pharmacy, Shenyang Pharmaceutical University, Shenyang, 110016, China
[b] School of Traditional Chinese Material Medica, Shenyang Pharmaceutical University, Shenyang, 110016, China
[c] Key Laboratory of Structure-Based Drug Design & Discovery of Ministry of Education, Shenyang Pharmaceutical University, Shenyang, 110016, China
[d] Health Science Center Department of Pharmacy, Shenzhen University, Shenzhen, Guangdong, 518118, China

ARTICLE INFO

Article history:
Received 21 October 2019
Received in revised form
27 April 2020
Accepted 20 May 2020
Available online 23 May 2020

Keywords:
Polygonum cuspidatum
Pulmonary fibrosis
TGF-β receptor type-I
Resveratrol
High resolution mass spectrometry
Molecular docking

ABSTRACT

Pulmonary fibrosis (PF) is an irreversible lung disease that is characterized by excessive scar tissue with a poor median survival rate of 2–3 years. The inhibition of transforming growth factor-β receptor type-I (TGF-β RI) by an appropriate drug may provide a promising strategy for the treatment of this disease. *Polygonum cuspidatum* (PC) is a well-known traditional Chinese herbal medicine which has an anti-PF effect. Accordingly, a combination of high resolution mass spectrometry with an in silico strategy was developed as a new method to search for potential chemical ingredients of PC that target the TGF-β RI. Based on this strategy, a total of 24 ingredients were identified. Then, absorption, distribution, metabolism, and excretion (ADME)-related properties were subsequently predicted to exclude compounds with potentially undesirable pharmacokinetics behaviour. Molecular docking studies on TGF-β RI were adopted to discover new PF inhibitors. Eventually, a compound that exists in PC known as resveratrol was proven to have excellent biological activity on TGF-β RI, with an IC_{50} of 2.211 μM in vitro. Furthermore, the complex formed through molecular docking was tested via molecular dynamics simulations, which revealed that resveratrol had strong interactions with residues of TGF-β RI. This study revealed that resveratrol has significant potential as a treatment for PF due to its ability to target TGF-β RI. In addition, this research demonstrated the exploration of natural products with excellent biological activities toward specific targets via high resolution mass spectrometry in combination with in silico technology is a promising strategy for the discovery of novel drugs.

1. Introduction

Pulmonary fibrosis (PF), an irreversible disease of the lung, causes normal lung tissue to be constantly replaced by fibroblasts or collagen, and eventually leads to death due to respiratory failure. Patients who are diagnosed with this disease have a poor median survival rate of 2–3 years [1]. Although the molecular mechanisms of PF have been studied in-depth, only a few effective drugs have been successfully developed to reverse PF [2]. Lung transplantation remains the most effective treatment for PF [3].

In contrast with the healing that occurs in healthy lungs, repetitive injuries to the lungs of PF patients can lead to abnormal activation of the epithelial-mesenchymal transition (EMT) process, which causes the formation of a pro-fibrotic environment [4]. The EMT process is regulated by numerous extracellular factors, among which transforming growth factor-β1 (TGF-β1) has long been regarded as a central mediator [5]. Specifically, activated TGF-β1 binds to its type II receptor, causing phosphorylation of TGF-β receptor type-I (TGF-β RI) to occur on cell membranes, which in turn activates an intracellular downstream signalling pathway to advance disease progression [6]. Serine/threonine protein kinase TGF-β RI is an attractive target in efforts to block the pro-fibrotic

Peer review under responsibility of Xi'an Jiaotong University.
* Corresponding author.
** Corresponding author.
E-mail addresses: cathybcc@szu.edu.cn (W. Bi), liuran8515@hotmail.com (R. Liu).

https://doi.org/10.1016/j.jpha.2020.05.007

effect of overexpressed TGF-β1. Small-molecule TGF-β RI inhibitors can modulate the EMT process that is mediated by the TGF-β signalling pathway, and have broad prospects in the treatment of PF. Thus far, several inhibitors targeting TGF-β RI have been developed for PF treatment, such as SD-208 [7] and SB-525334 [8]. However, the use of these inhibitors has been limited because of the potential cardiac toxicity [9].

Traditional Chinese medicine (TCM), which has a long history of disease prevention and treatment practice, has made a very positive contribution to human health and is a valuable resource [10]. Some single herbs and multiple-herb formulas exhibit benefits against PF, which demonstrates that natural products can potentially provide a rich supply of PF inhibitors [11,12]. *Polygonum cuspidatum* Sieb. et Zucc (PC), which is widely known as Huzhang in China, is one of the herbs included in the Chinese Pharmacopoeia [13]. A number of studies have shown that some active ingredients that exist in PC exhibit potential benefits against PF [14,15]. The multiple-herb formula Hu-qi-yin, which takes PC as the monarch, is composed of nine medicinal plants and is widely used as a remedy for PF in China [16]. It is apparent that PC, a well-established TCM, may provide a valuable resource in efforts to develop an effective treatment for PF.

In the past decade, natural products with excellent biological activity have offered important inspiration for the discovery and design of chemical drugs [17]. Among various research methods, virtual screening technology based on molecular docking has numerous advantages as a strategy for the exploration of the active chemical ingredients of TCM and their targets. At present, several natural products in PC have been reported to have anti-PF effects by regulating the TGF-β signalling pathway [15,18]. However, there have been no further investigations into the reasons why these natural products may trigger the inhibition of this signalling pathway, or to find their direct protein targets. More importantly, if the reasons for triggering this signalling pathway were found, these natural products may be identified as potential inhibitors of the specific protein targets. Thus, we took the key protein TGF-β RI in the TGF-β signalling pathway as an example, and offered a combination strategy of high resolution mass spectrometry and an in silico method to explore whether there are compounds that might be potential TGF-β RI inhibitors. The biological activity was tested to validate the results obtained via virtual screening, and molecular dynamics (MD) simulations of docking complexes were performed to provide insights into the mechanism of interaction between the screened inhibitor and TGF-β RI. The combination of high resolution mass spectrometry and an in silico method offered a feasible strategy to explore natural products with excellent biological activities toward specific therapeutic targets.

2. Materials and methods

2.1. Reagents and chemicals

HPLC-grade methanol was purchased from Thermo Fisher Scientific Inc. (Fair Lawn, NJ, USA). HPLC-grade formic acid was obtained from Tianjin Kemiou Chemical Reagent Co., Ltd. (Tianjin, China). Polydatin, resveratrol, and emodin were supplied by the National Institute for Food and Drug Control (Beijing, China). Emodin-8-*O*-glucoside, emodin-1-*O*-glucoside, physcion, and aloe-emodin were provided by Chengdu Chroma-Biotechnology Ltd. (Chengdu, China). Physcion-8-*O*-glucoside was obtained from Chengdu Pufei De Biotech Co., Ltd. (Chengdu, China). The purities of these reference compounds were all above 98.0%. The positive control drug SB-431542 (99.7% purity) was purchased from Bide Pharmatech Ltd. (Chengdu, China). Human recombinant TGF-β RI (catalogue number ICR8397Hu01) was obtained from ImmunoClone (Houston, TX, USA). Kinase-Glo Luminescent Kinase Assay (catalogue number V3771) was purchased from Promega (Madison, WI, USA). Distilled water was provided by Wahaha Company (Hangzhou, China). Adenosine triphosphate (ATP, catalogue number A7699) and all other reagents were acquired from Sigma-Aldrich (St. Louis, MO, USA).

PC was obtained from Tong-Ren-Tang TCM Store (Shenyang, China) and authenticated by Dr. Dong Wang (Shenyang Pharmaceutical University, Shenyang, China). The quantitative analysis of typical ingredients of PC was performed with an Agilent 1260 HPLC system (Santa Clara, CA, USA). The contents of polydatin, resveratrol, emodin-8-*O*-glucoside, and emodin in the sample prepared via the method described in Section 2.3 were found to be 0.7650%, 0.0640%, 0.5290%, and 0.0850% by weight. The analytical methods and their validation are provided in the Supplementary data.

2.2. Apparatus

2.2.1. Liquid chromatography (LC) system

LC analysis was performed with an Agilent 1260 infinity liquid chromatography system consisting of a quaternary pump, an autosampler, an on-line degasser, and a column temperature controller. Samples were separated on a Waters Cortecs T3 (2.1 mm × 100 mm, 2.7 μm; Waters, Milford, MA, USA) column at 30 °C. The mobile phase consisted of water containing 0.1% formic acid (A) and methanol (B) and the elution gradient was set by volume as follows: 20% B (0 min), 32% B (5 min), 37% B (7 min), 52% B (8 min), 100% B (15 min), and 100% B (20 min). The mobile phase flow rate was 0.4 mL/min with a sample injection volume of 2 μL.

2.2.2. Mass spectrometry (MS)

A Triple TOF 5600+ quadrupole time-of-flight tandem mass spectrometer (Sciex, Redwood City, CA, USA) was connected to the LC system via an electrospray ionization (ESI) interface and operated in the negative mode. The optimized parameters for the MS conditions were as follows: ion spray voltage, −4500 V; declustering potential (DP), 80 V; the turbo spray temperature, 550 °C; nebulizer gas (nitrogen), 50 psi; heater gas (nitrogen), 50 psi; and curtain gas (nitrogen), 30 psi. The scan range that was used in both the time-of-flight-mass spectrometry (TOF-MS) and time-of-flight tandem mass spectrometry (TOF-MS/MS) modes was *m/z* 100–800. In the TOF-MS mode, the collision energy (CE) was 10 eV. In the TOF-MS/MS mode, a typical information dependent acquisition (IDA) was used with a CE setting at 45 ± 15 eV. The collision gas was set at 15 psi.

2.3. Sample preparation

The standard solution was obtained by dissolving precisely weighed samples of emodin, emodin-8-*O*-glucoside, emodin-1-*O*-glucoside, physcion-8-*O*-glucoside, physcion, aloe-emodin, resveratrol, and polydatin in methanol.

The sample solution was extracted by refluxing powdered PC (0.1 g) in 25 mL of 70% aqueous methanol for 1 h, which was followed by centrifugation at 12,000 rpm for 5 min. The solution was filtered through 0.22 μm membranes prior to injection into the liquid chromatography-electrospray ionization quadrupole time-of-flight mass spectrometry (LC-ESI-QTOF-MS/MS) system.

2.4. Pharmacokinetic prediction

ADME is the four-letter abbreviation denoting absorption, distribution, metabolism, and excretion in pharmacokinetics. The ADME properties play a very significant role in the drug development process as poor pharmacokinetic properties are responsible

for the failure of most drugs in the clinical phase [19]. Computational methods have become a key tool that enables researchers to predict potentially undesirable ADME properties and to reduce the number of animal experiments [20]. In this study, three ADME-related properties including aqueous solubility, human intestinal absorption (HIA) levels, and cytochrome P450 2D6 enzyme (CYP2D6) binding levels, were employed to investigate the pharmacokinetic properties of chemical ingredients in PC by Discover Studio 3.0 software.

2.4.1. Aqueous solubility

By using 775 compounds as a training set, a model derived from a genetic partial least squares method was developed to predict the solubility of each compound in aqueous media at 25 °C [21]. Solubility is a particularly important property because it influences a drug's pharmacokinetic properties. A lower solubility can hinder the absorption and distribution of a compound, and often a special formulation or modification is required to enhance the solubility of an otherwise poorly soluble drug.

2.4.2. HIA levels

By using 182 well-absorbed compounds with actively transported molecules removed as a training set, a pattern recognition model based on calculations of logP and polar surface area (PSA) was developed [22]. The intestinal drug absorption is important for the oral drug delivery system, because the first step for obtaining a high oral bioavailability is to achieve a good absorption [23].

2.4.3. CYP2D6 binding levels

By using 151 compounds with known CYP2D6 inhibitions as a training set, an ensemble recursive partitioning model was developed to investigate whether or not a compound is likely to be a CYP2D6 inhibitor [24]. The cytochrome P450 family is composed of over 30 distinct isozymes, of which CYP2D6 accounts for less than 2% of the total content of P450 in the liver, but is responsible for 30% of all drug metabolisms [25,26]. Compounds that inhibit the activities of CYP2D6 can give rise to metabolic drug interaction (MDI), thus leading to an increase in the plasma concentration and promoting the abnormal elimination of other drugs that were simultaneously administered to a patient.

In this work, the compounds with solubility levels in the range of 2–4, a HIA of level 0, and a CYP2D6 binding value of "false" were selected for subsequent research, while others were ruled out. For comparison, the TGF-β RI targeted two known inhibitors, including galunisertib (in clinical phase 2/3) and vactosertib (in clinical phase 1), which were also subjected to ADME screening.

2.5. Molecular docking

The molecular docking was performed using Maestro 9.2 software. Meanwhile, MarvinSketch 16.4.25.0 software was used to draw two-dimensional (2D) structures of the determined ligands. Discover Studio 3.0 software was employed to accurately and efficiently acquire three-dimensional (3D) structures for computer analysis. The information regarding the crystal structures of TGF-β RI is deposited in the Protein Data Bank (PDB) (https://www.rcsb.org/) database (Table S3). The crystal structure with the PDB entry 6B8Y was downloaded for the molecular docking study because it offered the highest resolution and the highest reliability [27]. PyMol software was used to create high-quality images of the results.

The entire molecular docking process consisted of three steps: protein preparation, receptor grid generation, and ligand docking. Protein preparation was a process utilized to equip protein with a high-confidence structure that would be ideal for use. During this stage, hydrogen atoms were added, atomic charges were assigned, water molecules that were not involved in ligand binding were eliminated, and other relevant modifications were performed. In the next step, a grid box was generated by the prepared protein and its original ligand with the application of an OPLS_2005 force field. The active site of the grid box was defined with a 10 Å radius around the co-crystal ligand. During the last step, the compounds were imported into the active pocket for molecular docking studies under the extra precision (XP) mode. All other parameters were set as default. The accuracy of the docking was validated by redocking the original ligand after removal of the ligand from the ligand binding protein PDB file. The Root Mean Square Deviation (RMSD) [28]

Table 1
The chemical ingredients identified in *polygonum cuspidatum* (PC) via high performance liquid chromatography-quadrupole time-of-flight mass spectrometry (HPLC-QTOF-MS).

No.	Retention time (min)	$[M-H]^-$	Error (ppm)	Fragment ions (*m/z*)	Compounds
1	0.94	331.0671	−1.0	169.0135, 125.0242	6-*O*-galloylglucose
2	1.08	169.0143	0.6	125.0266	Gallic acid
3	1.45	577.1352	0.1	451.1009, 425.0872, 407.0767, 289.0725	Procyanidin B4
4	1.64	153.0193	0.9	108.0240, 109.0294	3,4-dihydroxybenzoic acid
5	2.25	289.0718	−0.4	245.0835, 203.0726, 109.0311	Catechin
6	3.91	729.1461	0.4	577.1400, 559.0866, 451.1035, 289.0717	Procyanidin-B-7-3-*O*-gallate
7	4.68	289.0718	−0.1	245.0806, 203.0719, 109.0305	Epicatechin
8	6.33	389.1242	−0.9	227.0728, 185.0624, 143.0517	Resveratroloside
9	7.12	441.0827	−1.7	289.0725, 245.0812, 205.0486	Epicatechin gallate
10	7.55	389.1242	−0.4	227.0727, 185.0611, 143.0505	Polydatin
11	10.19	541.1352	−0.6	313.0563, 227.0710, 169.0142, 151.0036, 125.0247	Resveratrol-4′-*O*-(6″-*O*-galloy)-glucoside
12	10.64	227.0714	0.4	185.0632, 143.0514	Resveratrol
13	11.96	431.0984	−0.2	269.0458, 225.0559	Emodin-1-*O*-glucoside
14	12.29	407.1348	−1.0	245.0815, 230.0581, 215.0347, 159.0451	Torachrysone-8-*O*-glucoside
15	12.37	431.0984	0.2	269.0458, 240.0437	Aloe-emodin-8-*O*-glucoside
16	12.41	299.0561	2.1	227.0453, 211.0404	Fallacinol
17	13.05	431.0984	−0.7	269.3377, 241.0493, 225.0540	Emodin-8-*O*-glucoside
18	13.16	449.1453	−1.0	245.0823, 230.0589, 215.0350	Torachryson-8-*O*-(6′-acetyl)-glucoside
19	13.79	445.1140	−1.0	283.0614, 268.0374, 240.0428	Physcion-8-*O*-glucoside
20	13.89	285.0405	0.7	268.0388, 257.0472, 229.0510, 224.0485, 211.0413	Citreorosein
21	14.27	487.1246	−0.9	283.0614, 268.0371, 240.0426	Physcion-8-*O*-(6′-acetyl)-glucoside
22	15.97	269.0456	1.0	241.0504, 225.0554, 182.0370	Emodin
23	16.55	509.1242	−0.6	254.0582	Palmidin
24	16.93	283.0612	−0.9	240.0430, 212.0468, 184.0508	Physcion

between the experimental and calculated structures was 0.299 Å in our docking program.

2.6. Validation of biological activity

The compound activity was assessed in an autophosphorylation assay based on the Kinase-Glo™ system and modified incubation conditions from those described in a previous report were adopted [6]. Specifically, TGF-β RI (20 nM) was first preincubated in 50 μL of Tris buffer (50 mM Tris, pH 7.5, 5 mM $MgCl_2$, 5 mM $MnCl_2$, 100 mM NaCl, 10 mM D,L-dithiothreitol) with different concentrations of compounds for 15 min at 37 °C. The reaction started with the addition of 3 μM ATP. After 20 min at 37 °C, phosphorylation was stopped via the addition of 50 μL of kinase-Glo plus reagent. The luminescence of each reaction mixture was measured by a Molecular Devices SpectraMax M2 (San Jose, CA, USA) system after 10 min of incubation. The results were calculated with GraphPad Prism 8 software.

2.7. MD simulations

The MD simulations was an effective tool that allowed us to simulate the allosteric process of proteins from the atomic level. The complex obtained from the docking experiment was introduced into Desmond v 3.8 software for the MD simulation. Simple point charged (SPC) waters were used as solvent molecules. An appropriate amount of Na^+ and Cl^- was added to the system to render the simulated system electrically neutral. Before the start of the simulation, the energy of the complex was minimized and subjected to a restrictive simulation in a normal volume and temperature (NVT) system with a gradual increase in temperature from 0 to 300 K. The MD simulations were conducted for 100 ns under a normal pressure and temperature (NPT) system.

3. Results and discussion

3.1. Compounds identified in PC

In order to obtain a more comprehensive analysis of the compounds in PC, the total ion chromatograms (TICs) obtained in both positive and negative modes were compared in this study and it was found that most compounds were more readily detected via the negative mode. Therefore, the negative mode was employed and as many as 24 compounds were identified (Table 1). HPLC chromatograms of blank solvent, mixed standard solution and sample

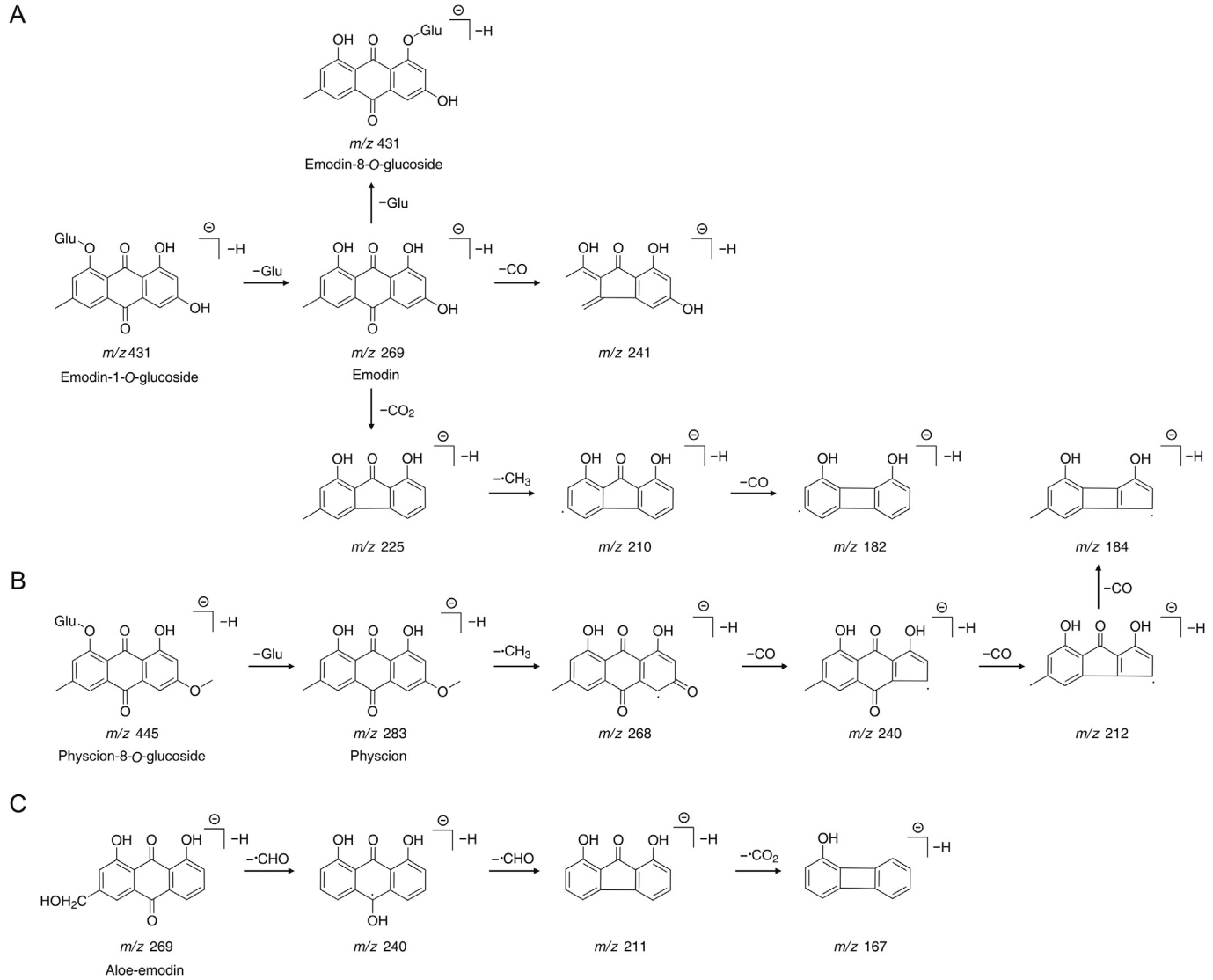

Fig. 1. The fragmentation pathways of selected anthraquinone reference compounds. (A) Emodin-8-*O*-glucoside, emodin-1-*O*-glucoside and emodin; (B) physcion-8-*O*-glucoside and physcion; and (C) aloe-emodin.

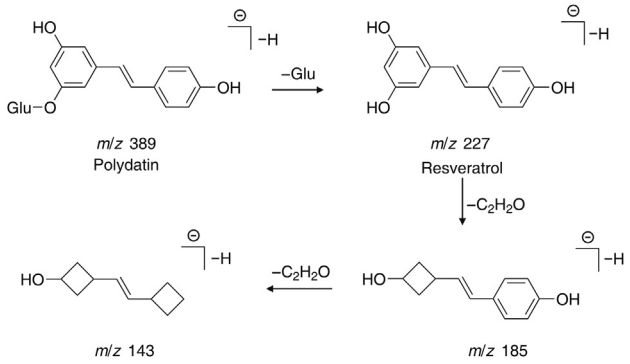

Fig. 2. The fragmentation pathways of the stilbene reference compounds resveratrol and polydatin.

solution are shown in Fig. S1. All of the identified compounds had well-defined chemical structures (Fig. S2). The TIC is shown in negative mode in Fig. S3. An acceptable accuracy error was used as the threshold that reached as low as 3 ppm in this study.

According to previous reports, anthraquinones and stilbenes are the main components of PC. Standard compounds of the representative species from these two families were infused to summarize the fragmentation regularity from ESI-MS.

3.1.1. The fragmentation regularity and identification of anthraquinones

Emodin-8-*O*-glucoside, emodin-1-*O*-glucoside, emodin, physcion-8-*O*-glucoside, physcion, and aloe-emodin were respectively analyzed to obtain the diagnostic product ions. Emodin is the aglycone of emodin-8-*O*-glucopyranoside and emodin-1-*O*-glucoside, and therefore their $[M-H]^-$ ions differ by *m/z* 162. Emodin yielded a $[M-H]^-$ ion at *m/z* 269, of which the MS^2 product ions were observed at *m/z* 241 and *m/z* 225 due to the neutral loss of CO and CO_2, respectively. The ion at *m/z* 225 formed an ion at *m/z* 210 by losing a $\cdot CH_3$ radical, and then further produced an ion at *m/z* 182 via the loss of CO. Emodin-8-*O*-glucoside and emodin-1-*O*-glucoside were distinguished based on their retention times because they had similar product ions. Physcion is the aglycone of physcion-8-*O*-glucoside, so a difference of *m/z* 162 was observed between the $[M-H]^-$ ions of these compounds. The $[M-H]^-$ ion at *m/z* 283 yielded the ion at /*z* 268 via the loss of $\cdot CH_3$, which further eliminated CO units multiple times to produce ions at *m/z* 240, 212, and 184. Aloe-emodin and emodin showed the same molecular composition, with a $[M-H]^-$ ion at *m/z* 269 corresponding to both of these compounds, but their product ions were completely different. The $[M-H]^-$ ion at *m/z* 269 of aloe-emodin lost $\cdot CH_3$ radicals twice, thus yielding the ions at *m/z* 240 and 211. The $[M-H]^-$ ion at *m/z* 211 further eliminated CO_2 to produce an ion at *m/z* 167. The fragmentation pathways of selected anthraquinone reference compounds are shown in Fig. 1. Based on the analysis of fragment ions and comparison with literature reports [29,30], ten anthraquinone derivatives were identified, including various anthraquinones as well as anthraquinone glycoside.

3.1.2. The fragmentation regularity and identification of stilbenes

Two typical stilbenes of polydatin and its aglycon resveratrol that exist in PC were investigated. The $[M-H]^-$ ion of polydatin observed at *m/z* 389 formed an ion at *m/z* 227 via the elimination of

Table 2
ADME-related properties of 24 chemical ingredients found in *polygonum cuspidatum* (PC) and those of known inhibitors.

No.	Compounds	Aqueous solubility		HIA			CYP2D6 binding	
		Score	Level[a]	ALogP98	PSA	Level[b]	Score	Level[c]
Chemical ingredients in PC								
1	6-*O*-galloylglucose	−0.406	2–4	−1.474	189.240	3	−3.732	False
2	Gallic acid	−0.491	2–4	0.733	100.562	0	−8.128	False
3	Procyanidin B4	−7.402	1	3.565	226.015	3	3.071	Ture
4	3,4-dihydroxybenzoic acid	−0.633	2–4	0.975	79.747	0	−7.004	False
5	Catechin	−2.445	2–4	2.021	113.007	0	0.679	True
6	Procyanidin-B-7-3-*O*-gallate	−12.158	0	4.882	293.877	3	0.337	True
7	Epicatechin	−2.444	2–4	2.021	113.007	0	0.679	True
8	Resveratroloside	−2.674	2–4	1.288	160.054	3	−11.564	False
9	Epicatechin gallate	−5.538	2–4	3.339	180.869	3	0.354	True
10	Polydatin	−2.072	2–4	1.160	142.753	1	−8.305	False
11	Resveratrol-4′-O-(6″-*O*-galloyl)-glucoside	−4.895	2–4	2.447	210.615	3	−8.980	False
12	Resveratrol	−2.560	2–4	3.090	62.446	0	−3.019	False
13	Emodin-1-*O*-glucoside	−3.294	2–4	0.638	177.354	3	−5.239	False
14	Torachrysone-8-*O*-glucoside	−2.347	2–4	0.534	148.168	2	−5.738	False
15	Aloe-emodin-8-*O*-glucoside	−2.398	2–4	−0.210	177.354	3	−5.485	False
16	Fallacinol	−2.682	2–4	1.703	105.978	0	−2.175	False
17	Emodin-8-*O*-glucoside	−3.277	2–4	0.638	177.354	3	−5.541	False
18	Torachryson-8-*O*-(6′-acetyl)-glucoside	−2.727	2–4	0.913	153.583	3	−7.023	False
19	Physcion-8-*O*-glucoside	−3.263	2–4	0.864	165.469	3	−6.420	False
20	Citreorosein	−2.325	2–4	1.477	117.863	0	−2.408	False
21	Physcion-8-*O*-(6′-acetyl)-glucoside	−3.500	2–4	1.243	170.884	3	−7.985	False
22	Emodin	−3.312	2–4	2.568	97.048	0	−3.154	False
23	Palmidin	−6.177	1	4.648	159.494	3	−0.255	False
24	Physcion	−3.761	2–4	2.794	85.162	0	−3.582	False
Known inhibitors								
1	Galunisertib	−4.995	2–4	2.600	81.038	0	−2.731	False
2	Vactosertib	−5.769	2–4	3.882	78.257	0	−3.445	False

[a, b, c] refer to the meanings of different ADME properties at different levels for screening drug-like compounds.

[a] Solubility levels of 0, 1, 2–4, and 5 denote solubility levels that are as follows: insoluble (with no marketed drugs existing in this range); only slightly soluble (but with some marketed drugs existing in this range); in the drug-like category; extremely soluble (but without many marketed drugs existing in this solubility range), respectively.

[b] HIA levels of 0, 1, 2, and 3 indicate that the absorption levels are well, moderate, poor, and very poor, respectively.

[c] A CYP2D6 level of "false" indicates that the respective compound is unlikely to inhibit the cytochrome P450 2D6 enzyme.

ADME: absorption, distribution, metabolism, and excretion; HIA: human intestinal absorption; PSA: polar surface area; CYP2D6: cytochrome P450 2D6 enzyme.

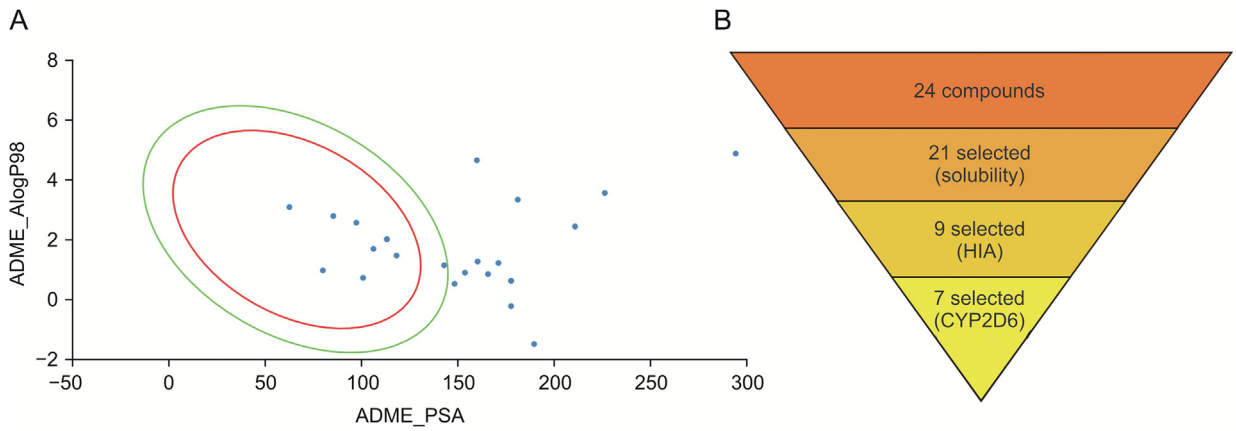

Fig. 3. Prediction of the ADME properties. (A) Prediction of the 24 chemical ingredients in *polygonum cuspidatum* (PC) for the human intestinal absorption (HIA) based on polar surface area (PSA) and ALogP98. Green and red regions represent 99% and 95% confidence ellipsoids for HIA, respectively. Dark blue dots depict various chemical ingredients. (B) The steps of absorption, distribution, metabolism, and excretion (ADME)-based screening of 24 chemical ingredients in PC.

a glycosyl residue. The product ion *m/z* 227, also the $[M-H]^-$ ion of resveratrol, formed ions at *m/z* 185 and *m/z* 143 by losing C_2H_2O in a sequential manner. The fragmentation pathway of selected stilbene reference compounds is shown in Fig. 2. The fragmentation regularity of these stilbenes references was mainly due to the loss of C_2H_2O units with a mass of 42. Based on the analysis of fragment ions and comparison with literature reports [31,32], four stilbene derivatives were identified, including resveratrol and three glycoside derivatives.

3.1.3. Identification of other compounds

Aside from the anthraquinones and stilbenes mentioned above, several compounds including six gallates/tannins, two naphthalenes, and two other compounds, were also detected in this study. Their probable structures were characterized by comparing their respective fragment ions with literature data [32–34].

3.2. Prediction of the ADME properties

All 24 of the chemical ingredients were subjected to screening for ADME-related properties (Table 2). Among these, four anthraquinone compounds, one stilbene compound, and two other compounds were selected for subsequent investigation, including gallic acid, 3,4-dihydroxybenzoic acid, resveratrol, fallacinol, citreosein, emodin, and physcion. Solubility levels of 0, 1, 2–4, and 5 respectively correspond to solubility levels that were as follows: too low for further consideration; slightly soluble (but with some marketed drugs existing in this range); solubilities in the drug-like category; extremely high solubility but without many marketed drugs existing in that particular range, respectively [21]. Based on these solubility parameters, 21 ingredients of PC were found to be in the drug-like category. Meanwhile, HIA levels of 0, 1, 2, and 3 reflect absorption levels to be well, moderate, poor, and very poor, respectively [35]. It is noteworthy that among the 21 remaining ingredients, only 9 were found to fulfil the set criteria at 99% confidence limit ellipses based on the set criteria of PSA and AlogP98 (Fig. 3A). The area enclosed by the ellipse is a prediction that the corresponding compounds would be well-absorbed. Most of the excluded compounds were observed to be glycosides, which was possibly due to glucosyl release by the microbial metabolism in the intestine, causing the structures of the glycosides to break down during absorption [36]. A CYP2D6 level of "false" was predicted as non-inhibitors and the two compounds catechin and epicatechin were ruled out due to their predicted CYP2D6 inhibitory activity. Fig. 3B summarizes the various steps involved in the screening of chemical ingredients of PC with suitable ADME properties.

Table 3
The docking results between existing inhibitors with transforming growth factor-β receptor type-I (TGF-β RI).

No.	PDB code	Resolution (Å)	Hydrogen bonding	Ref.
1	1VJY	1.70	HID_283	[6]
2	6B8Y	1.65	HID_283, ASP_351	[27]
3	3TZM	3.70	HID_283, LYS_232	[37]
4	5USQ	2.55	HID_283	[38]
5	2X7O	2.00	HID_283, ASP_281	[39]

PDB: Protein Data Bank.

3.3. Molecular docking analysis

Five inhibitors possessing experimental structures with inhibitory behaviour toward TGF-β RI were analyzed to evaluate how they acted on the target [6,27,37–39] (Table 3). Their protein-ligand interaction diagrams are in Fig. S4. The results indicated that the interaction between small molecule inhibitors and TGF-β RI was consistent. All of the investigated inhibitors formed hydrogen bonds with HID_283, which could be considered as an active site

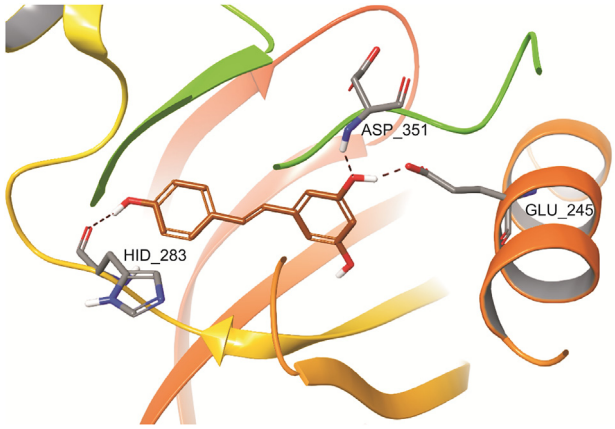

Fig. 4. The predicted binding model between resveratrol and transforming growth factor-β receptor type-I (TGF-β RI). The protein is depicted as ribbons. Small molecules and contact residues are depicted as brown and grey sticks, respectively. The brown dotted line illustrates the hydrogen bonds.

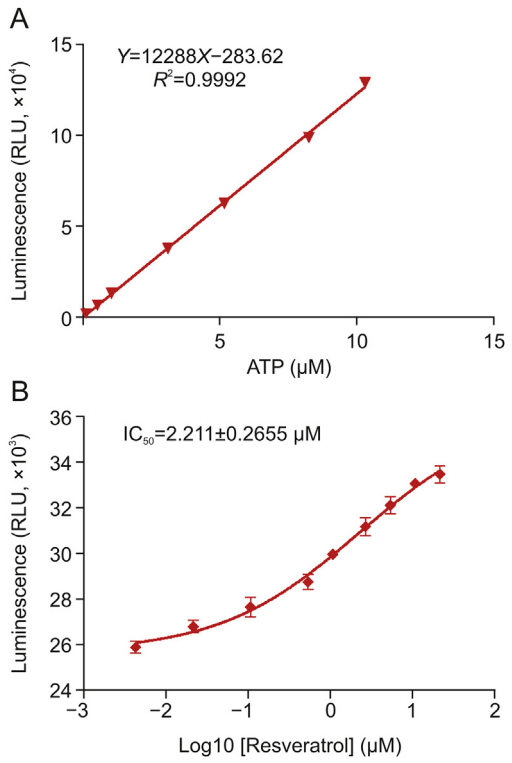

Fig. 5. Data obtained via biological activity validation in an autophosphorylation assay based on the Kinase-Glo™ system. (A) A linear relationship between the luminescence signal and the concentration of ATP over a range from 0 to 10 μM. The correlation coefficient (R^2) was 0.9992 for this range. (B) A dose-dependent inhibition curve of resveratrol on transforming growth factor-β receptor type-I (TGF-β RI) activity. The IC_{50} value of resveratrol was 2.211 ± 0.2655 μM.

TGF-β RI. It is worth mentioning that residues 281–283 in TGF-β RI were in a region normally occupied by the adenine ring of ATP [6], suggesting that certain compounds inhibited TGF-β RI by occupying the ATP binding site.

Molecular docking studies were effectively conducted to screen potent inhibitors targeting TGF-β RI. The binding energy and hydrogen-bonding residues are presented in Table S4. All 7 compounds had high binding energies (<−8 kcal/mol), which might be a false positive result caused by the presence of more polar groups in these compounds [40]. In other words, the binding site targeted by most molecules with multiple polar groups was not actually the active site. It is noteworthy that resveratrol showed a similar mode of action to those of existing inhibitors (Fig. 4), suggesting that it could bind with the active site of TGF-β RI to inhibit its activity.

3.4. Biological activity validation

We first demonstrated a linear relationship between the luminescence signal and the concentration of ATP (Fig. 5A). The TGF-β RI inhibitor SB-431542 [37] was selected as a positive control to measure the level of inhibition exhibited by test compound. The IC_{50} of SB-431542 in the established Kinase-Glo™ system was 1.568 ± 0.1959 μM.

Different concentrations of resveratrol (20 μM, 10 μM, 5 μM, 2.5 μM, 1 μM, 500 nM, 100 nM, 25 nM, and 5 nM) were respectively added to the reaction system to measure the kinase autophosphorylation activity of TGF-β RI. As shown in Fig. 5B, as the concentration of resveratrol in the reaction system gradually increased, the phosphorylation of the kinase diminished, resulting in a gradual increase in the remaining ATP concentration. As a promising inhibitor targeting TGF-β RI, the IC_{50} of resveratrol was 2.211 ± 0.2655 μM, which was close to the IC_{50} of the positive control.

3.5. MD simulations of docked complexes

As shown in Fig. S5A, the RMSD value of the protein backbone fluctuated slightly during the first 50 ns and remained stable at approximately 2.2 Å until the end of the simulation. In addition, the RMSD value of the ligand-protein complex fluctuated significantly during the first 55 ns, but decreased to an equilibrium value after

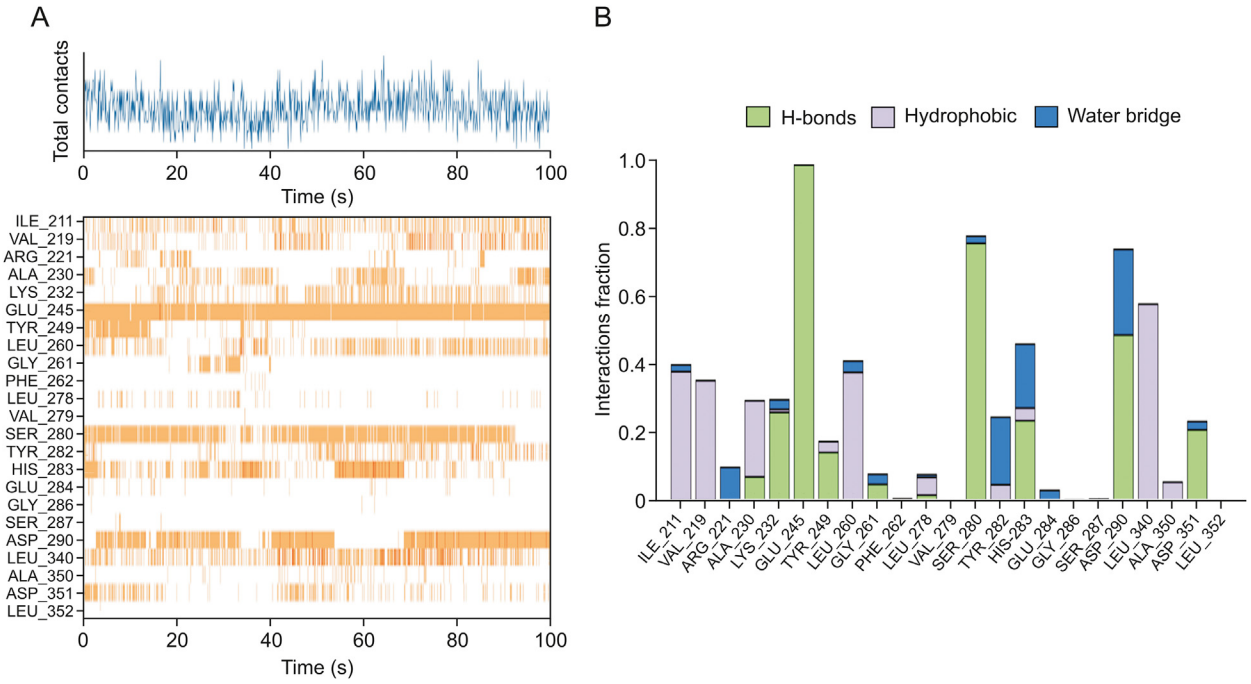

Fig. 6. Results of molecular dynamics simulations of docking complexes. (A) A timeline representation and (B) a normalized stacked bar chart for protein-ligand contact interaction over the trajectory of the entire simulation.

55 ns. These results indicated that the system reached equilibrium after 55 ns. The root-mean-square fluctuation (RMSF) was plotted to characterize local changes of the protein chain (Fig. S5B), and the protein residues that fluctuated the most were displayed in the form of peaks. Three types of protein-ligand interactions were found, including hydrogen bonds, as well as hydrophobic and water bridges. The interaction between resveratrol and TGF-β RI was shown with the use of a timeline representation and as a normalized stacked bar chart (Fig. 6). GLU_245, SER_280, and ASP_290 exhibited strong hydrogen bonding interactions with time occupancies of 97%, 69% and 48%, respectively, during the whole simulation. Meanwhile, LYS_232, HIS_283, and ASP_351 could also form a significant degree of hydrogen bonds, accounting for values of 25%, 22%, and 20%, respectively. The nonpolar residues LEU_340, LEU_260, ILE_211, and VAL_219 could form strong hydrophobic interactions, accounting for values of 57.3%, 37.4%, 37.6% and 35.0%, respectively. ASP_290, TYR_282, and HIS_283 offered important water bridging interactions accounting for percentages of 35.0%, 19.7% and 18.6%, respectively. All of the interactions described above formed the basis for the biological activity of resveratrol. The findings obtained via the MD simulation were consistent with the docking results.

3.6. Identification of resveratrol as a potential TGF-β RI inhibitor

The identification of active compounds that focus on therapeutic targets is of great significance in the field of drug development. TGF-β RI has been viewed as an attractive drug target for the treatment of PF [9]. The curative effect of PC on PF has been widely recognized during its long history as a TCM. After preliminary screening, resveratrol came to our attention as a potential lead compound that could inhibit TGF-β RI. In our study, three ADME-related parameters, namely, aqueous solubility, HIA, and CYP2D6 binding, were employed to investigate pharmacokinetic characteristics of resveratrol. Nevertheless, pharmacokinetic behaviour is also related to other numerous properties. Beyond the three properties that we have chosen, resveratrol was reported to have an absorption rate reaching as high as 75%, but a bioavailability of less than 1% [41], which was mainly due to its rapid metabolism in the liver. The good absorption behaviour was consistent with our prediction (with HIA level of 0). Meantime, the poor bioavailability caused by rapid metabolism was no longer an issue, as it could be effectively addressed in various ways, such as the use of nanoformulations, bioenhancers, and phytochemical combinations [42].

Notably, it has been reported that resveratrol can trigger the inhibition of the TGF-β signalling pathway involved in the development of anti-PF [18]. However, this is the first time that the mechanism of resveratrol-triggered inhibition of this signalling pathway has been explored. The exploration of mechanisms based on specific therapeutic targets can provide significant contributions resulting in the discovery of lead compounds in drug development. We have not only confirmed that resveratrol exhibits biological activity by targeting TGF-β RI, but also explored the binding mode between resveratrol and the residues of TGF-β RI via an in silico strategy. The results obtained from molecular docking studies and MD simulations suggest that resveratrol may exert its inhibitory activity by competitively binding to the ATP binding sites of TGF-β RI. In the future, more activity verification experiments will be performed to study the interactions between resveratrol and TGF-β RI.

4. Conclusion

In the study, we established a comprehensive approach that combined high-resolution mass spectrometry with an in silico strategy to investigate potential active ingredients of PC that target the TGF-β RI. A total of 24 chemical ingredients were identified, and a compound database of PC was established on a preliminary basis. In silico methods were effectively used to predict the ADME-related properties of the chemical ingredients while molecular docking studies were also conducted, which revealed that resveratrol has potential inhibitory activity that targets TGF-β RI with an IC_{50} of 2.211 μM in vitro. Moreover, the results obtained from MD simulations indicated that hydrogen bonds as well as hydrophobic and water bridges contributed to the interactions between resveratrol and TGF-β RI. In summary, resveratrol was discovered to be a promising lead compound for the development of TGF-β RI inhibitors. This work will help to accelerate the development of clinical drugs for the treatment of PF.

CRediT author statement

Huarong Xu: Conceptualization, Methodology; **Jiameng Qu:** Software, Data curation, Writing - Original draft preparation; **Jian Wang:** Supervision, Writing - Reviewing and Editing; **Kefei Han**: Visualization, Investigation; **Qing Li**: Supervision, Writing - Reviewing and Editing; **Wenchuan Bi**: Supervision, Validation; **Ran Liu:** Conceptualization, Writing - Reviewing and Editing.

Declaration of competing interest

The authors declare that there are no conflicts of interest.

Acknowledgments

This work was financially supported by the National Natural Science Foundation of China (Grant Nos.: 81703463 and 81603277), the National Key R&D Program of China (Grant No.: U1508220), the Liaoning Distinguished Professor Project for Qing Li, and the Doctoral Scientific Research Foundation of Liaoning Province (Grant No.: 20170520199).

Appendix A. Supplementary data

Supplementary data related to this article can be found at https://doi.org/10.1016/j.jpha.2020.05.007.

References

[1] A. Duck, L.G. Spencer, S. Bailey, et al., Perceptions, experiences and needs of patients with idiopathic pulmonary fibrosis, J. Adv. Nurs. 71 (2014) 1055–1065.
[2] M. Myllärniemi, R. Kaarteenaho, Pharmacological treatment of idiopathic pulmonary fibrosis - preclinical and clinical studies of pirfenidone, nintedanib, and *N*-acetylcysteine, Eur. Clin. Respir. J. 2 (2015), 26385.
[3] A. Kumar, S.G. Kapnadak, R.E. Girgis, et al., Lung transplantation in idiopathic pulmonary fibrosis, Expet Rev. Respir. Med. 12 (2018) 375–385.
[4] H. Kage, Z. Borok, EMT and interstitial lung disease: A mysterious relationship, Curr. Opin. Pulm. Med. 18 (2012) 517–523.
[5] L.C. Li, D.L. Li, L. Xu, et al., High-mobility group box 1 mediates epithelial-to-mesenchymal transition in pulmonary fibrosis involving transforming growth factor-beta1/Smad2/3 Signaling, J. Pharmacol. Exp. Therapeut. 354 (2015) 302–309.
[6] F. Gellibert, J. Woolven, M.H. Fouchet, et al., Identification of 1,5-naphthyridine derivatives as a novel series of potent and selective TGF-β type I receptor inhibitors, J. Med. Chem. 47 (2004) 4494–4506.
[7] P. Bonniaud, P.J. Margetts, K. Ask, et al., TGF-β and Smad3 signaling link inflammation to chronic fibrogenesis, J. Immunol. 175 (2005) 5390–5395.
[8] H. Higashiyama, D. Yoshimoto, T. Kaise, et al., Inhibition of activin receptor-like kinase 5 attenuates Bleomycin-induced pulmonary fibrosis, Exp. Mol. Pathol. 83 (2007) 39–46.
[9] H.I. Adamali, T.M. Maher, Current and novel drug therapies for idiopathic pulmonary fibrosis, Drug Des. Dev. Ther. 6 (2012) 261–272.
[10] W.X. Ding, J.Y. Gu, L. Cao, et al., Traditional Chinese herbs as chemical resource library for drug discovery of anti-infective and anti-inflammatory, J. Ethnopharmacol. 155 (2014) 589–598.

[11] L.C. Li, L.D. Kan, Traditional Chinese medicine for pulmonary fibrosis therapy: Progress and future prospects, J. Ethnopharmacol. 198 (2017) 45–63.
[12] S. Hosseini, M. Imenshahidi, H. Hosseinzadeh, et al., Effects of plant extracts and bioactive compounds on attenuation of bleomycin-induced pulmonary fibrosis, Biomed. Pharmacother. 107 (2018) 1454–1465.
[13] W. Peng, R.X. Qin, X.L. Li, et al., Botany, phytochemistry, pharmacology, and potential application of *Polygonum cuspidatum* Sieb. et Zucc.: A review, J. Ethnopharmacol. 148 (2013) 729–745.
[14] J. Wang, F. He, L.Q. Chen, et al., Resveratrol inhibits pulmonary fibrosis by regulating miR-21 through MAPK/AP-1 pathways, Biomed. Pharmacother. 105 (2018) 37–44.
[15] R.J. Guan, X. Wang, X.M. Zhao, et al., Emodin ameliorates bleomycin-induced pulmonary fibrosis in rats by suppressing epithelial-mesenchymal transition and fibroblast activation, Sci. Rep. 6 (2016), 35696.
[16] X.M. Zhou, G.C. Zhang, J.X. Li, et al., Inhibitory effects of Hu-qi-yin on the bleomycin-induced pulmonary fibrosis in rats, J. Ethnopharmacol. 111 (2007) 255–264.
[17] T. Rodrigues, D. Reker, P. Schneider, et al., Counting on natural products for drug design, Nat. Chem. 8 (2016) 531–541.
[18] Y.Q. Zhang, Y.J. Liu, Y.F. Mao, et al., Resveratrol ameliorates lipopolysaccharide-induced epithelial mesenchymal transition and pulmonary fibrosis through suppression of oxidative stress and transforming growth factor-beta1 signaling, Clin. Nutr. 34 (2015) 752–760.
[19] A. Cheng, D.J. Diller, S.L. Dixon, et al., Computation of the physio-chemical properties and data mining of large molecular collections, J. Comput. Chem. 23 (2001) 172–183.
[20] G. Moroy, V.Y. Martiny, P. Vayer, et al., Toward in silico structure-based ADMET prediction in drug discovery, Drug Discov. Today 17 (2012) 44–55.
[21] A. Cheng, K.M. Merz Jr, Prediction of aqueous solubility of a diverse set of compounds using quantitative structure-property relationships, J. Med. Chem. 46 (2003) 3572–3580.
[22] W.J. Egan, K.M. Merz Jr, J.J. Baldwin, Prediction of drug absorption using multivariate statistics, J. Med. Chem. 43 (2000) 3867–3877.
[23] T.J. Hou, J.M. Wang, W. Zhang, et al., ADME evaluation in drug discovery. 7. prediction of oral absorption by correlation and classification, J. Chem. Inf. Model. 47 (2007) 208–218.
[24] R.G. Susnow, S.L. Dixon, Use of robust classification techniques for the prediction of human cytochrome P4502D6 inhibition, J. Chem. Inf. Comput. Sci. 43 (2003) 3867–3877.
[25] T. Shimada, H. Yamazaki, M. Mimura, et al., Interindividual variations in human liver cytochrome P-450 enzymes involved in the oxidation of drugs, carcinogens and toxic chemicals: Studies with liver microsomes of 30 Japanese and 30 Caucasians, J. Pharmacol. Exp. Therapeut. 270 (1994) 414–423.
[26] G.W.M. Chang, P.C.A. Kam, The physiological and pharmacological roles of cytochrome P450 isoenzymes, Anaesthesia 54 (1999) 42–50.
[27] L.S. Harikrishnan, J. Warrier, A.J. Tebben, et al., Heterobicyclic inhibitors of transforming growth factor beta receptor I (TGFbetaRI), Bioorg. Med. Chem. 26 (2018) 1026–1034.
[28] A.E. Lohning, S.M. Levonis, B. Williams-Noonan, et al., A practical guide to molecular docking and homology modelling for medicinal chemists, Curr. Top. Med. Chem. 17 (2017) 2023–2040.
[29] F.Y. Gao, T.T. Zhou, Y.S. Hu, et al., Cyclodextrin-based ultrasonic-assisted microwave extraction and HPLC-PDA-ESI-ITMS^n separation and identification of hydrophilic andhydrophobic components of *Polygonum cuspidatum*: A green, rapidand effective process, Ind. Crop. Prod. 80 (2016) 59–69.
[30] L. Wang, M. Sang, E. Liu, et al., Rapid profiling and pharmacokinetic studies of major compounds in crude extract from Polygonum multiflorum by UHPLC-Q-TOF-MS and UPLC-MS/MS, J. Pharm. Biomed. Anal. 140 (2017) 45–61.
[31] L.Y. Xie, B.W. Bolling, Characterisation of stilbenes in California almonds *(Prunus dulcis)* by UHPLC–MS, Food Chem. 148 (2014) 300–306.
[32] X.H. Qiu, J. Zhang, Z.H. Huang, et al., Profiling of phenolic constituents in Polygonum multiflorum Thunb. by combination of ultra-high-pressure liquid chromatography with linear ion trap-Orbitrap mass spectrometry, J. Chromatogr. A 1292 (2013) 121–131.
[33] F.W. Ma, X.J. Gong, X. Zhou, et al., An UHPLC–MS/MS method for simultaneous quantification of gallic acid and protocatechuic acid in rat plasma after oral administration of Polygonum capitatum extract and its application to pharmacokinetics, J. Ethnopharmacol. 162 (2015) 377–383.
[34] Z.H. Huang, Y. Xu, Q. Wang, et al., Metabolism and mutual biotransformations of anthraquinones and anthrones in rhubarb by human intestinal flora using UPLC-Q-TOF/MS, J. Chromatogr. B 1104 (2019) 59–66.
[35] S. Singh, T. Das, M. Awasthi, et al., DNA topoisomerase-directed anticancerous alkaloids: ADMET-based screening, molecular docking, and dynamics simulation, Biotechnol. Appl. Biochem. 63 (2016) 125–137.
[36] L. Hanske, G. Loh, S. Sczesny, et al., The bioavailability of apigenin-7-glucoside is influenced by human intestinal microbiota in rats, J. Nutr. 139 (2009) 1095–1102.
[37] A.A. Ogunjimi, E. Zeqiraj, D.F. Ceccarelli, et al., Structural basis for specificity of TGFbeta family receptor small molecule inhibitors, Cell. Signal. 24 (2012) 476–483.
[38] M. Sabat, H.X. Wang, N. Scorah, et al., Design, synthesis and optimization of 7-substituted-pyrazolo[4,3-b] pyridine ALK5 (activin receptor-like kinase 5) inhibitors, Bioorg. Med. Chem. Lett. 27 (2017) 1955–1961.
[39] G.J. Roth, A. Heckel, T. Brandl, et al., Design, synthesis, and evaluation of indolinones as inhibitors of the transforming growth factor beta receptor I (TGFbetaRI), J. Med. Chem. 53 (2010) 7287–7295.
[40] R.S. Ferreira, A. Simeonov, A. Jadhav, et al., Complementarity between a docking and a high-throughput screen in discovering new cruzain inhibitors, J. Med. Chem. 53 (2010) 4891–4905.
[41] M. Rotches-Ribalta, C. Andres-Lacueva, R. Estruch, et al., Pharmacokinetics of resveratrol metabolic profile in healthy humans after moderate consumption of red wine and grape extract tablets, Pharmacol. Res. 66 (2012) 375–382.
[42] N. Pannu, A. Bhatnagar, Resveratrol: From enhanced biosynthesis and bioavailability to multitargeting chronic diseases, Biomed. Pharmacother. 109 (2019) 2237–2251.